Hydrol. Earth Syst. Sci. Discuss., 8, 10739–10780, 2011
www.hydrol-earth-syst-sci-discuss.net/8/10739/2011/
doi:10.5194/hessd-8-10739-2011

Hydrology and Earth System Sciences Discussions

Extreme runoff response to short-duration convective rainfall in South-West Germany

V. Ruiz-Villanueva[1], M. Borga[2], D. Zoccatelli[2], L. Marchi[3], E. Gaume[4], U. Ehret[5], and E. Zehe[5]

[1]Natural Hazards Division, Geological Survey of Spain (IGME), Madrid, Spain
[2]Department of Land and Agroforest Environment, University of Padova, Legnaro, Italy
[3]CNR IRPI, Padova, Italy
[4]LUNAM Université, IFSTTAR, GER, 44341 Bouguenais, France
[5]Institut für Wasser und Gewässerentwicklung, Bereich Hydrologie KIT Karlsruhe, Germany

Received: 22 November 2011 – Accepted: 22 November 2011 – Published: 7 December 2011

Correspondence to: V. Ruiz-Villanueva (v.ruiz@igme.es)

Published by Copernicus Publications on behalf of the European Geosciences Union.

Abstract

The 2 June 2008 flood-producing storm on the Starzel river basin in South-West Germany is examined as a prototype for organized convective systems that dominate the upper tail of the precipitation frequency distribution and are likely responsible for the flash flood peaks in this region. The availability of high-resolution rainfall estimates from radar observations and a rain gauge network, together with indirect peak discharge estimates from a detailed post-event survey, provides the opportunity to study the hydrometeorological and hydrological mechanisms associated with this extreme storm and the ensuing flood. Radar-derived rainfall, streamgauge data and indirect estimates of peak discharges are used along with a distributed hydrologic model to reconstruct hydrographs at multiple locations. The influence of storm structure, evolution and motion on the modeled flood hydrograph is examined by using the "spatial moments of catchment rainfall" (Zoccatelli et al., 2011). It is shown that downbasin storm motion had a noticeable impact on flood peak magnitude. Small runoff ratios (less than 20 %) characterized the runoff response. The flood response can be reasonably well reproduced with the distributed hydrological model, using high resolution rainfall observations and model parameters calibrated at a river section which includes most of the area impacted by the storm.

1 Introduction

Analyses of inventories of flash floods in Europe have outlined seasonality effects and associated space-time scales in the distribution of these events across different European regions (Gaume et al., 2009; Marchi et al., 2010). According to these analyses, flash floods in the Mediterranean region (Italy, France and Catalonia) mostly occur in the autumn months, whereas events in the inland Continental region (Romania, Austria and Slovakia) tend to occur in the summer months, revealing different climatic forcing. Consistent with the seasonality effect, these analyses have shown that the

HESSD
8, 10739–10780, 2011

spatial extent and duration of the events is smaller for the Continental events compared to those occurring in the Mediterranean region. Even though the flash flood regime is generally more intense in the Mediterranean Region than in the Continental areas, flash floods occurring in the belt from Southern Germany to Romania play a specific role in the regional flood hydrology at small drainage areas (less than 100 km^2). Organised convective systems dominate the upper tail of the precipitation frequency distributions for short duration rainfall and are likely responsible for the flood peaks at small drainage areas in this region (Parajka et al., 2010). However, they are not prominently represented in flood frequency analyses for most stream gauging stations, even those with relatively long records. Flash floods are spatially-limited, locally rare events whose observation and monitoring is challenging given the available hydrometeorological networks (Carpenter et al., 2007; Borga et al., 2008; Smith et al., 2011; Brauer et al., 2011).

The recognition of the poor observability of flash floods has stimulated in the last decade the development of a focused monitoring methodology, which involves post-flood surveys, use of weather radar observation re-analyses and hydrological modelling (Costa and Jarrett, 2008; Borga et al., 2008; Gaume and Borga, 2008; Brauer et al., 2011). The implementation of this observation strategy has led to an improved characterisation of flash floods, both at the individual event scale (Hicks et al., 2005; Delrieu et al., 2005) and at the regional, multi-event scale (Costa and Jarrett, 2008; Gaume et al., 2009). Statistical regional procedures have been developed which may explicitly incorporate data from post-flood surveys to improve the estimation of extreme quantiles (Gaume et al., 2010). Ongoing research focuses on understanding how the data generated by this observational methodology may be used to discriminate between various hypotheses of runoff generation under flash flood conditions (Braud et al., 2010; Bonnifait et al., 2009), to test flash flood forecasting models (Norbiato et al., 2008; Versini et al., 2010) and to identify patterns of predictability (Blöschl, 2006).

In this paper, we examine the hydrometeorology and hydrology of an extreme flood in the Starzel catchment at Rangendingen (a 120 km^2 sub-basin of the Neckar river

HESSD
8, 10739–10780, 2011

system in South-Western Germany, Fig. 1), through analyses of the 2 June 2008 storm and flood. As an "end member" in the flood response spectrum at small drainage areas, analyses of Starzel response provide insights into the processes that produce extreme floods in small-medium size catchments in South-Western Germany. The 2 June 2008 flood in the Starzel river basin, similar to other extreme floods in the region, was produced by an organized system of thunderstorms. The storm produced large rainfall rates over the Starzel River catchment for a period of approximately 1 h 30 min and claimed the lives of three people. Estimates of the related rainfall event are based on volume scan reflectivity observations from two C-band weather radars operated by the German Weather Service (DWD) (Fig. 1). The rainfall estimates are used to characterise the structure and motion of the flash flood-producing storm and as an input to a distributed hydrological model for flood simulation.

A detailed post-flood survey was carried out in the period 10–14 November 2008 by an international team of experts. The field work included indirect estimation of peak discharges from flood marks (Lumbroso and Gaume, 2011) and documentation of the time evolution of the flood by means of information collected from eyewitnesses of the flood and local authorities. Overall, this has made it possible to depict a spatially-detailed pattern of flash-flood response along the stream network.

These observations are used together with high-resolution rainfall observations derived from radar and rain gauge observations and a distributed hydrologic model to reconstruct the event over various sub-basins and to check the consistency between rainfall estimates and indirect estimates of peak discharges. Indirect flood peak observations and simulations from the hydrological model are examined to assess the flood scale water balance and the runoff ratios. Finally, hydrologic modeling analyses are used to examine the dependence of flood response in the Starzel River on the spatial pattern of rainfall and storm motion. For this purpose, we use the method devised by Zoccatelli et al. (2011) based on the Spatial Moments of Catchment Rainfall.

HESSD
8, 10739–10780, 2011

2 The study area and its flood regime

The catchment of the Starzel river closed at Rangendingen (Fig. 1), which includes the area most severely affected by the flash flood of 2 June 2008, covers an area of 120 km^2. The elevation ranges from 419 to 954 m a.s.l., (average 644 m) and the mean slope is 12 %.

The catchment consists mainly of Jurassic sedimentary rocks, predominantly limestone, marls and claystone. Karst topography including fissures, sinkholes and caverns, is locally observed on the very eastern portions of the catchment, where limestone outcrops. Three main land use classes can be found in the catchment (Fig. 2): forest, agriculture and urban areas. Coniferous, mixed and deciduous forests cover most of basin slopes. Agricultural areas mostly consist of arable land, orchards and meadows. Three major urban areas are present in the valley floor: Jungingen (1.416 inhabitants), Hechingen (19.386 inhabitants) and Rangendingen (5.400 inhabitants).

According to long term data (1961–1990) recorded in Hechingen, average annual precipitation is 836 mm, with maxima in summer (from June to August); mean annual temperature is 8.3 °C, with minimum in January (−0.5 °C) and maximum in July (17.3 °C). The Starzel river catchment is part of the Neckar river system (Fig. 1). As shown by the relief map in Fig. 1b, it is situated at the edge of a Karst plateau named Schwäbische Alb. In the catchments along this edge, runoff production is influenced by karst effects caused by the Schwäbische Alb in the South. Also, the rim of the plateau is a typical spot for the triggering of convective uplift, which facilitates thunderstorm formation and for orographic rainfall enhancement. Annual rainfall along the rim lies at 900–1000 mm a^{-1}.

Estimates of the 2 June 2008 flood peak at Rangendingen range between 125 and 175 m^3 s^{-1}, i.e. from 1.0 to 1.5 m^3 (s^{-1} km^2), with a central value of 150 m^3 s^{-1}. In order to provide a context for the Starzel flash flood, we examined the flood hydrology of the catchments along the Schwäbische Alb rim. The analysis of regional extreme floods is based on data from 15 stream gauges, namely peak discharge of the three highest

HESSD
8, 10739–10780, 2011

recorded floods and 2-yr and 100-yr peak discharge statistics derived from stream-gauge measurements provided by the local water authorities. The catchments considered in the analysis were selected to be similar in size to the Starzel at Rangendingen (120 km^2), with areas ranging from 29 to 331 km^2. A total of 498 yr of peak flow observations is included in the overall regional sample, with a mean record length of 33 yr. The recurrence period of the three highest recorded flood events for each catchment range from 2-yr to >100-yr floods (more than 70 % are larger than 10-yr floods) (Fig. 3). These data provide a representative sample of extreme floods in the region. The information about the climatology of extreme precipitation is provided in the form of gridded (8.4 km) rainfall amounts for various durations (5 min–72 h) and return periods derived from raingauge statistics from the KOSTRA project (DWD, 1997).

The three highest recorded flood events at each of the 15 gauges are characterized according to the month of flood occurrence. Almost 75 % of the floods occur predominantly in the period May–August. The Starzel event of June 2008 is therefore representative in this region with respect to occurrence season. In fact, the three highest recorded floods at gauge Rangendingen, in operation since 1991, all occurred during this season (the other two largest floods occurred on 11 August 2002 and 21 June 2007). From an historical perspective, the largest flood in the region for which information is reported (albeit not in the form of a systematic record) occurred on 4–7 June 1895 in a catchment close to the Starzel river: the Eyach river basin at Balingen (128 km^2). The event consisted of three individual flood events that occurred on 4, 5 and 7 June 1895 each caused by intense thunderstorms totaling around 200 mm rainfall. In the days before the flood, substantial rainfall occurred, bringing the catchment to saturation. The reported peak discharge at Balingen is 350 $m^3 s^{-1}$, i.e. 2.7 $m^3 (s^{-1} km^2)$; the event claimed the lives of 40 people. According to the available regional flood frequency analyses, this flood peak exceeded 1000 yr return period (which is around 210 $m^3 s^{-1}$ for this catchment). A second catastrophic flood is reported for the Echaz catchment (133 km^2, near the Starzel basin) on 20 May 1906, with 135 $m^3 s^{-1}$. Overall, this shows the relevance of floods triggered by organized

HESSD
8, 10739–10780, 2011

systems of short, convective events for the study region, mainly occurring during late spring/summer season.

3 The flash flood of 2 June 2008

The rainstorm that triggered the flash flood of the Starzel River was part of a sequence of mesoscale precipitation systems (called Hilal) which occurred from 28 May to 2 June 2008 covering most of Western Germany. The Hilal organised system of thunderstorms formed along a stationary air mass boundary separating warm, moist Mediterranean air in the southwest from dry air in the northeast. The first system occurred on 28 May and was focused on Mid-West Germany (city of Dortmund), about 800 km North-West from the Starzel area. A second system occurred on 29–30 May, causing flooding in Luxembourg, Rhineland-Palatinate, and North Rhine-Westphalia. On the evening of 2 June, torrential storms led to flash flooding and inundation in Baden-Württemberg, with extreme rain intensities in parts of the Neckar basin. The Starzel catchment closed at Rangendingen was struck by the flood. The storm was very localised in space and characterised by strong spatial gradients and motion. The soil moisture conditions at the start of the event were relatively wet, given the precipitation in the previous days. The month of May 2008 was not particularly wet, with a rain depth measured in Hechingen equal to 85.1 mm, to be contrasted with a climatological 1961–1990 mean of 108.2 mm. However, more than half the monthly rain was concentrated in the last two days, as a consequence of the system of MCSs which characterized the period 28 May–2 June 2008. The flood was not associated with landsliding or debris flow, due to both the morphological characteristics of the catchment (with relatively short hillslopes) and the short character of the rain event which likely prevented the formation of the high pore water pressure required for slope instability. Only a few shallow slope failures and landslides were documented on the catchment area most impacted by the storm close to the town of Jungingen.

HESSD
8, 10739–10780, 2011

The Starzel river flows through the towns of Jungingen, Hechingen and Rangendingen, which were flooded with damage to roads, buildings and infrastructures; three people died as a consequence of the flood in Jungingen and in Hechingen.

4 Rainfall estimation and analyses

4.1 Rainfall data and spatial distribution

Radar and rain gauge observations were used to derive rainfall fields for the 2 June 2008 storm. The rainfall observation resources include two volume-scanning Doppler C-band radar located at Türkheim and Feldberg (Fig. 1), about 60 and 90 km off the study watershed, respectivley. The region impacted by the storm has a limited extension: only 4 hourly rain gauges could be used to check the radar-based estimates (Fig. 1). Data from the original volume scan data (which include 18 elevations, with time resolution of 5 min, and spatial resolution of 250 m in range by 1.0 degree in azimuth) were made available by DWD for radar rainfall estimation. This enabled the application of an integrated set of procedures, aiming at detecting and correcting the following errors: (i) partial beam occlusion; (ii) signal attenuation; (iii) vertical profile of reflectivity (VPR), (iv) radar hardware miscalibration. The correction procedures are described in detail by Bouilloud et al. (2010) for a different case study; a summary is provided below. Due to the extremely high rain rates, and the characteristics of the weather radar, specific attention was paid to the correction of the signal attenuation by means of the Mountain Reference Technique (MRT, hereinafter) (Delrieu et al., 2000). By applying the MRT, maximum path integrated attenuation (PIA, hereinafter) between 8 and 14 dB were measured for path-averaged rain rates between 10 and 15 $mm\,h^{-1}$ over a 50-km path. By considering the PIA constraint equation, the MRT allowed estimation of an effective radar calibration correction factor, assuming a drop size distribution model and the subsequent reflectivity-rain rate-attenuation relationships to be known. At each time step, the radar observations from either Türkheim and Feldberg

HESSD
8, 10739–10780, 2011

were used depending on the computed attenuation. Due to the presence of hail, a rain-rate threshold (hail cap) parameter was also imposed. Besides signal attenuation, screening effects were quantified using a numerical model of radar beam propagation in the atmosphere and the terrain model of the region. The vertical structure of reflectivity was modelled with the normalized apparent VPR estimated over the whole radar volume. The final step of the processing chain consisted of generating rainfall accumulation from the instantaneous surface rainfall rate estimation. To account for the bias, the final rainfall accumulations were scaled with a bias factor, computed by comparing the adjusted radar estimated and the raingauge values at the event aggregation scale.

Radar-rainfall estimates obtained in this way were evaluated by comparing them with rain gauge observations (which were considered as reference values) at the hourly aggregation scales (Fig. 4). The comparison was carried out in terms of Mean Absolute Error (equal to 0.48) and Correlation Coefficient (equal to 0.90), showing the quality of these estimates even with respect to results reported in other studies (Zanon et al., 2010).

Even though the radar estimates and raingauge measurement compare well, the uncertainties in reproducing fine features of the highly variable precipitation pattern need to be acknowledged. This is mainly related to the difficulties arising with the adjustment for the signal attenuation effects, which were particularly severe for this event.

The spatial distribution of the event-cumulated rainfall depth over the catchment is reported in Fig. 5, which shows that the largest rainfall amounts are localised on the central and lower portions of the catchment, with very large values over the right-hand tributaries.

The distribution of exceedance areas, i.e. the areas over which various rain thresholds were exceeded, is reported in Fig. 6, which shows that the most important rainfall amounts, exceeding 100 mm, impacted just around 30 % of the catchment.

Measuring rainfall for storms that produce extreme localised floods is fraught by large uncertainties. The 2 June 2008 flood provides a useful illustration of this uncertainty.

HESSD
8, 10739–10780, 2011

Information concerning the amount and the timing of the strong rainfall was collected by a weather amateur resident in Jungingen (Mr. Heizelmann). Mr. Heizelmann's rain gauge is located on a fence 1.5 m high in his garden and is appropriately located for a reasonably accurate measurement of rainfall. According to his observations, the rain amount exceeded 240 mm in 55 min. This rain amount is significantly higher than the highest radar estimates, which points to uncertainty either on the adjustment of the radar estimates or on the accuracy of the rain measures by the local observer. The value of 240 mm in 55 min is an extreme rainfall depth, which can be compared to the world record accumulation of 305 mm in 42 min recorded in Holt, Montana, on 22 June 1947. The rain observations by Mr. Heizelmann could not be validated and have not been used in this work but are reported as an indication of the potential uncertainties in rainfall estimation for extreme convective events.

The analysis of the mean areal rainfall depth over the basin at Ragendingen provides a value of 85.6mm for the entire storm event, and of 55.5 mm for the 90 min corresponding to highest intensities. A statistical analysis based on the KOSTRA methodology (DWD, 2006) shows that the observed short-term rainfall corresponds to a 100-yr recurrence interval. However, the recurrence interval of the entire event (85,6 mm in 10 h) is more extreme. The 100-yr rainfall of 9 h duration according to DWD (2006) amounts to 63.6 mm, which corresponds to 67.6 mm for 10 h. Examination of the quantiles corresponding to 1000-yr recurrence interval indicates that the rainfall was well beyond a 100-yr, but below a 1000-yr event. This corresponds also to the return period of the field-estimated discharge.

4.2 Space-time rainfall variability and storm motion

The spatial and temporal rainfall characteristics are examined here by using the spatial moments of catchment rainfall (Zoccatelli et al., 2011). As a detailed description of the method and of its assumptions is reported in Zoccatelli et al. (2010), only an outline of the method is given here. With these statistics, rainfall spatial variability is examined relative to a distance metric imposed by the flow distance, i.e. the distance along the drainage path from a generic point within the basin to the outlet of the basin drainage

HESSD
8, 10739–10780, 2011

network. The use of the flow distance is motivated by the observation that runoff routing imposes an effective averaging of spatial rainfall excess across locations with equal routing time, in spite of the inherent spatial variability. When hydrodynamic dispersion and variations in runoff propagation celerities can be neglected, the flow distance may be used a s a surrogate for runoff travel time. The first and second order scaled spatial moments of catchment rainfall at time t, indicated with $\delta_1(t)$ and $\delta_2(t)$ respectively, are computed as follows:

$$\delta_1(t) = \frac{|A|^{-1}\int_A r(x,y,t)d(x,y)dA}{|A|^{-1}\int_A r(x,y,t)dA\,|A|^{-1}\int_A d(x,y)dA}$$
$$\delta_2(t) = \frac{|A|^{-1}\int_A r(x,y,t)\left[d(x,y)-\delta_1(t)d_{\text{ave}}\right]^2 dA}{|A|^{-1}\int_A r(x,y,t)dA\,|A|^{-1}\int_A \left[d(x,y)-d_{\text{ave}}\right]^2 dA} \quad (1)$$

where $r(x,y,t)$ is the rainfall rate at position (x,y) in the basin and time t, $d(x,y)$ is the flow distance, d_{ave} is the mean value of the flow distance over the basin and A is the basin area.

Accordingly with these definitions, the first scaled moment δ_1 represents the ratio between the mean rainfall weighted flow distance and the product of the mean areal rainfall rate and the mean value of the flow distance. The second scaled moment δ_2 represents the ratio of the rainfall-weighted variance of the flow distances and the product of the mean areal rainfall rate and the variance of the flow distances.

A spatial rainfall distribution either concentrated close to the position of mean flow distance or spatially uniform results in values of δ_1 close to 1. A value of δ_1 less than one indicates that rainfall is distributed towards the basin outlet, whereas a value greater than one indicates that rainfall is distributed towards the headwaters.

In a similar way, a spatially uniform rainfall distribution results in values of δ_2 close to 1. A value of δ_2 less than one indicates that rainfall has a unimodal concentration along the flow distances. A value greater than one indicates indicate cases of multimodal rainfall distributions.

HESSD
8, 10739–10780, 2011

Equation (1) can also be extended to describe the spatial rainfall organization corresponding to the cumulated rainfall over a certain time period T_s (e.g. a storm event), obtaining the statistics termed Δ_1 and Δ_2, respectively.

Zoccatelli et al. (2011) showed that it is possible to relate the values of Δ_1 and Δ_2 with the shape of the hydrograph. A less-than-one value of Δ_1 (which means that rainfall is concentrated towards the outlet) results in an anticipation of the mean hydrograph time with respect to the same hydrograph obtained by a spatially uniform storm. A greater-than-one value of Δ_1 (which means that rainfall is concentrated towards the headwater) results in a delay of the mean hydrograph time. The value of Δ_2 influences the shape of the flood hydrograph. The values of Δ_2 are greater than zero and take the value of one when the rainfall field is spatially uniform. Less than one values corresponds to a rainfall field which is spatially concentrated anywhere in the basin. In the less frequent cases when the rainfall field has a bimodal spatial distribution, with concentration both at the headwaters and at the outlet of the catchment, the values of Δ_2 are greater than one. In general the effect of decreasing the value of Δ_2 is to increase the flood peak (Zoccatelli et al., 2011).

Based on the formulation of the spatial moment relationships in Eq. (1), it is possible to derive an expression for the effective storm velocity as it is filtered by the drainage properties of the catchment. Zoccatelli et al. (2011) have shown that the resulting catchment scale storm velocity (V_s) is defined as:

$$V_s = g_1 \frac{\mathrm{cov}_t[T, \delta_1(t) w(t)]}{\mathrm{var}[T]} - g_1 \frac{\mathrm{cov}_t[T, w(t)]}{\mathrm{var}[T]} \Delta_1 \quad (2)$$

where T is time, $\mathrm{cov}_t[]$ denotes the temporal covariance operator and var[ ] denotes the variance. The rainfall weigths $w(t)$ are obtained as the ratio between the instantaneous mean areal rainfall rate and the mean value of the basin-averaged rainfall rate over the storm event.

Equation (2) shows that the storm velocity is defined as the difference between the slope terms of two linear regressions with time (Zoccatelli et al., 2011). The first slope term is estimated based on the space-time regression between weighted scaled first

HESSD
8, 10739–10780, 2011

moments and time, and the second term is based on the regression between weights and time. Conceptually, this means that storm motion may produce changes both in the rainfall centroid coordinate and in the mean areal rainfall values. Both are taken into account in the estimation of the catchment scale storm velocity. For the case of temporally uniform mean areal rainfall, $w(t)$ is constant and the value of V_s depends only on the evolution in time of the position of the rainfall centroid along the flow distance coordinate. In the opposite case, if there is only temporal variation of the mean areal rainfall and no motion ($\delta_1(t)$ is constant), the two slope terms will be equal in value and opposite in sign, which means that the V_s will be equal to zero. Note that the sign of the velocity is positive (negative) for the case of upstream (downstream) storm motion.

Results from the analysis with the spatial moments of catchment rainfall are reported in Fig. 7. The temporal distribution of mean areal rainfall shows two main storms. The first, with 15-min peak rain rate around 25 mm h^{-1}, lasted between 16:00 to 17:15 CET; the second storm was much more intense (peak rain rate around 50 mm h^{-1} at 15 min time intervals) and occurred between 18:00 and 19:30. During the second storm rain rates exceeded 20 mm h^{-1} on more than 75 % of the catchment.

Examination of the time series of $\delta_1(t)$ and $\delta_2(t)$ shows that during the first storm the precipitation was mainly concentrated around the catchment geomorphological centroid, with a peaky spatial distribution. Around 17:15–17:30 CET rain rates decrease and the rainfall centroid shifts suddenly to the headwaters of the catchment. The second storm is less localised, with a centroid moving regularly from the far periphery of the basin to positions close to the outlet. This originates a downbasin catchment scale storm motion, with a velocity around 0.5–0.6 m s^{-1} in the first part of the second storm. This velocity is around 30 % of that estimated for the stream flow velocity, showing that it is far from being optimal for peak flow generation (Ogden et al., 1995). However, this may have added to the severity of the storm, giving rise to a stronger flood peak than that expected purely based on the spatial distribution of rain depth and intensities.

HESSD
8, 10739–10780, 2011

5 The post event survey and indirect peak discharge estimation

The Starzel river catchment is equipped with a streamgauge station at Rangendingen, but the recorded maximum stage during the event exceeds by far the stages for which direct current meter measurements are available. The streamgauge and parts of the floodplain upstream the section were inundated during the flood, so that the maximum recorded stage value (corresponding to around 80 $m^3 s^{-1}$ according to the current rating curve) was considered to underestimate high discharge, especially the flood peak. An indirect peak flood estimate, based on analysis of flood traces in non-overflooded river sections upstream the streamgauge station was carried out just after the flood by the Baden-Württenberg hydrological services (M. Moser, local Water Authority, personal communication, 2008). The indirect peak flood estimate provided an assessment of peak flow between 120 and 155 $m^3 s^{-1}$.

A post-flood survey campaign (denoted IPEC, Intensive Post-Event Campaign, hereinafter) was organised in the period 10–14 November 2008 with the main objective to examine the spatially distributed flood response properties to the storm. The field work included surveying of high water marks (HWM), water surface slope and cross-sectional geometry at multiple sites along the river network. These data were used to estimate indirectly the flood peaks by means of hydraulic equations. The IPEC was organised in the frame of the European Project HYDRATE (http://www.hydrate.tesaf.unipd.it), funded by the EU Commission, Sixth Framework Programme (Borga et al., 2011), with the collaboration of local authorities. Even though 6 months passed between the date of the flood and that of the field survey, the HWM were still clearly recognisable. Also, the stream bed morphology (which is typical of a bedrock river in many sectors of the channel network) was not severely modified by the flood. This gives confidence in using the post-flood geometry for peak flood computation. Thirty-three cross-sections were surveyed during the field campaign and peak discharges were assessed using the slope-conveyance method (Gaume and Borga, 2008; Marchi et al., 2009). The location of the cross sections is reported in Fig. 2. The discharge

HESSD
8, 10739–10780, 2011

estimates help mapping the flood responses along the Starzel River, its main tributary the Reichenbach, as well as the contribution of parts of their tributaries. A selection of the original cross section data, concerning 17 sections which are at reasonable distance each other along the same river reach, thus providing relatively independent information, is reported in Table 1.

Indirect peak discharge estimates are potentially affected by a range of uncertainties, which may be induced by errors in HWM assessment and in the choice of roughness coefficients, in the use of the post-flood geometry and its survey, in the assumptions concerning the energy line slope, and by possibly undetected backwater effects.

Uncertainty ranges reported in Table 1 account for the uncertainty in the selection of the Manning roughness parameter and in the energy slope estimation, in the form of a 95 % uncertainty range. This leads to underestimate the actual uncertainty in indirect peak discharge estimation. However, a complete quantitative treatment of the uncertainty involved in the survey is not a central objective of this paper and will be reported in future works.

Despite the mentioned sources of uncertainties, the values reported in Table 1 appear to be consistent with each-other. The peak discharge increases steadily from the headwaters to Jungingen. Downstream Jungingen the field-observed peak discharges are around 120–170 $m^3 s^{-1}$ in the reaches upstream Rangendingen, with a value in Sect. 3 which appears relatively higher than downstream sections even accounting for uncertainty. The inundation of the town of Hechingen may have had an attenuating effect on the flood wave of the Starzel river. The peak discharge indirect estimates in Ragendingen corresponds to a return time around 100 yr (which is estimated at 160 $m^3 s^{-1}$ for a basin area of 120 km^2 in the study region).

The chronology of the start of overflooding and of the peak stage was also investigated based on the witnesses' interviews and movies recorded by eye-witnesses of the flood. In Jungingen, the sequence of the events was reconstructed as follows (timing is given here in local solar time, i.e. CET): "Around 18:15, river level in Jungingen rose from bankfull to peak, with around 1.2–1.5 of water in the streets. The river reached

HESSD
8, 10739–10780, 2011

the peak at around 18:45, maintaining the level for around 20 min. Between 20:00 and 20:30 the river stage reduces to the embankment level". Overall this agrees with the information provided by the rainfall sequence.

6 Rainfall-runoff analysis

6.1 Relationships between field-derived peak flows and rain properties

The relationship between the distribution of the field-observed unit peak discharges and the properties of the rainfall forcing is reported in Fig. 8. For each surveyed basin, three basin-averaged rainfall characteristics are reported and analysed: the event cumulated rainfall, the maximum hourly rainfall and the maximum 30-min rainfall. Not surprisingly, the highest values of unit peak discharge are observed in the smallest catchments (area less than 10 km^2). In particular, the sections 12, 26 and 37 (all corresponding to catchment areas in the range of 1.1 to 2.1 km^2), located in the area affected by the most intense rainfalls, are characterised by very high values of specific discharge. These values are around 5.8 m^3 (s^{-1} km^2) for Sections 12 and 37 and around 12 m^3 (s^{-1} km^2) for Section 26. These are extreme values for the study area.

The pattern of the relations between precipitation and unit peak discharge is very similar for cumulated storm precipitation and 1-h maximum rainfall intensity. This can be ascribed to the close correlation between total event rainfall and 1-h maximum rainfall, which becomes poor when 30-min rainfall is considered (Fig. 9a, b). For instance, catchments 10, 12, 25 and 26 have very similar event-cumulated rain depths and max 1-h rain depths. However, max 30-min rain depths are less than 90 mm h^{-1} for catchments 10 and 12, and close to 130 mm h^{-1} for catchments 25 and 26.

Small catchments induce a large scatter in the relationship presented in Fig. 8. For instance, catchments 25 and 26 are characterised by very similar rain depths (127.2 and 127.3 mm, respectively) and intensities, they are very close to each other and have very similar size (around 2 km^2). However, field-estimated flood peak from catchment

HESSD
8, 10739–10780, 2011

26 is almost three times that reported for catchment 25. Even the field-estimated flow velocity is very similar (Table 1), which means that the main difference between the two estimates is in the surveyed HWM and section geometry. Possible explanations for such differences includes the difficulty to correctly estimate the watershed area for these small catchments. The watershed area was estimated based on a digital elevation model of 90 m grid size, which is adequate for the main objectives of this study and for the size of the Starzel basin, but is rather rough for basin size as small as 1 km^2.

When examination of the values reported in Fig. 8 is limited to catchments larger than 10 km^2, a relatively good relationship is found between specific unit peak flow and the rain event-accumulation and 1 h maximum. However, the linear pattern is lost when 30 min maximum rain is considered, showing that this rain property bears limited influence on catchment response for basins larger than 10 km^2. This is not a surprising result, since the time of concentration of watersheds exceeding 10 km^2 is higher than 30 min, according to the analyses carried out in the study.

6.2 Rainfall-runoff modelling

Hydrologic response to the June 2008 storm is examined by using a spatially distributed hydrologic model. Three main objectives are pursued with this modelling application: (i) analysis of the accuracy in simulating the spatially distributed runoff response when applying model calibration at the outlet sections in Rangendingen and Jungingen; (ii) examination of the hydrologic consistency of the field-derived peak discharges; and (iii) assessment of the impact of the rainfall variability on the simulated flood hydrographs at Rangendingen.

The hydrological model is described in detail in Zanon et al. (2010) and only an outline is provided here. The discharge $Q(t)$ is computed by the model at any location along the river network as follows:

HESSD
8, 10739–10780, 2011

$$Q(t) = \iint_A q[x,y,t-\tau(x,y)]dxdy \quad (3)$$

where A_s [L^2] indicates the area draining to the specified outlet location, $\tau(x,y)$ [T] is the routing time from the location (x,y) to the outlet of the basin specified by the region and $q(x,y,t)$ is the runoff rate at time t and location x,y. The runoff rate is computed from the rainfall rate $r(x,y,t)$ using the Green-Ampt infiltration model with moisture redistribution (*Ogden and Saghafian*, 1997). The routing time $\tau(x,y)$ is computed as

$$\tau(x,y) = \frac{d_h(x,y)}{v_h} + \frac{d_c(x,y)}{v_c} \quad (4)$$

where $d_h(x,y)$is the distance from the generic point x,y to the channel network following the steepest descent path, $d_c(x,y)$ is the length of the subsequent drainage path through streams down to the watershed outlet. v_h and v_c are two invariant hillslope and channel flood celerities, respectively. The model includes also a linear conceptual reservoir for base flow modeling (Borga et al., 2007). The reservoir input is provided by the infiltrated rate computed based on the Green-Ampt method.

The model requires estimation of seven calibration parameters: the channelization support area (A_s), two kinematic parameters (v_h and v_c), the three soil hydraulic parameters used by the Green-Ampt method and the time constant of the conceptual linear reservoir. The model was implemented over the Starzel catchment at 15-min time step and using a 90 m grid size cell for the description of landscape morphology and soil properties. The most sensitive model parameters (saturated hydraulic conductivity and flow velocity parameters) were calibrated based on the peak flood estimated in Rangendingen and on the information concerning the chronology of the flood (discharge raising time and peak flow time) collected in Rangendingen and in Jungingen by using the methodology followed by Zanon et al. (2010). Accordingly, the channelization support area (A_s) is found equal to 2.43 ha, v_c is equal to 3 m s^{-1} and v_h is equal to 0.05 m s^{-1}. The value of channel celerity agrees well with field based observations

HESSD
8, 10739–10780, 2011

reported in Table 1. The value of saturated hydraulic conductivity was set equal to 10 mm h^{-1} in the urbanized area in the floodplains and to 20–40 mm h^{-1} on the areas characterized by agriculture and forest land use, respectively. The initial conditions in the Green-Ampt model were set to fit the observed initial discharge in Rangendingen. As such, they were relatively wet.

Results from the model application are reported for the catchment at Rangendingen (Fig. 10) and at Jungingen (Fig. 11). As expected, the flood hydrograph simulated in Rangendingen shows large discrepancies with respect to the one derived on the basis of the observed streamgauge data. This is related to the overflowing of the cross section and of the floodplain upstream the section. Owing to this reason, the simulated flood peak is anticipated. The chronology of the flood peak agrees with accounts reported by witnesses. The hydrograph simulated at Jungingen shows a satisfactory agreement with the chronology of the flood as reported in the account of witnesses about the start of the bank overtopping, the time of flood peak and the end of the river bank overtopping (Fig. 11). For both catchments, the simulated flood peak is included in the range of indirect peak discharge estimates reported on the basis of the post-flood survey.

Flood water balance data are reported in Table 2 for the catchments closed at Jungingen and at Rangendingen. These data, obtained by using the field-validated model simulations, show that the runoff ratio is very low. In spite of the wet antecedent soil moisture conditions and of the high rain rates and accumulations, runoff depth is just a small percentage of the rainfall volume, ranging from 0.13 to 0.16. These values are significantly lower than those reported by Marchi et al. (2010) for similar catchments and hydro-climatic conditions, with Alpine and Continental flash flood events characterized by mean values of runoff ratio equal to 0.20 and 0.30, respectively. Uncertainties in rainfall estimates and model simulations may affect the findings about the runoff ratio. However, these values are in the range of those reported for specific small and medium size catchments and for events characterized by short rain durations in Continental Europe (Zoccatelli et al., 2010). When considering these events, it is apparent that the

HESSD
8, 10739–10780, 2011

rainfall duration is an important control on runoff ratio, with initial losses accounting for an important contribution to the overall losses.

The hydrological model was applied to simulate peak discharges over the 17 sub-catchments where IPEC post-flood surveys are available. Corresponding results are provided in Fig. 12a, b for the peak discharges and the unit peak discharges, respectively. In both figures, the uncertainty ranges for field-derived peak discharges are shown together with the central values. The results reported in Fig. 12a show a good fit between simulated and observed peak discharges, with a Nash-Sutcliffe efficiency equal to 0.91. Overall, this suggests that the hydrological model provides a reasonably good description of the spatial distribution of the runoff response to the extreme rain, at least for catchments exceeding a threshold area of around 10 km^2. The success in the hydrological simulation may be ascribed to the strong forcing of the rainfall, which was estimated with relatively good accuracy for the study basin and was likely able to overcome other sources of spatial variability (such as those related to soil/geological properties) which are more difficult to determine. When considering these results, one should take into account that this representation tends to weight more the large discharges. Analysis of the results obtained for the unit peak discharges (Fig. 12b) permits closer examination of the simulations for the smaller basins. The examination allows one to isolate the behavior of the tributaries corresponding to sites 37, 12 and 26, all corresponding to very small catchments (Table 1), where simulated peak values substantially underestimate the very high specific values obtained by the IPEC. For site 25, the model overestimates significantly the field-derived peak discharge. Several sources of uncertainties may be considered to explain the difficulties in reproducing the flood for these small basins. These sources of uncertainty certainly include possible errors in rainfall estimation, as well as difficulties in delineating the actual extension of the catchments and errors in indirect peak discharge estimation.

Model simulated peak values were also used to examine the hydrologic consistency of the field-derived peak discharges. With this analysis, the field-derived peak discharges whose uncertainty range does not include the simulated peak discharges are

HESSD
8, 10739–10780, 2011

screened out, as these are considered inconsistent with the rainfall space-time distribution and the model-based flood response description. Sites flagged as inconsistent should be closely scrutinised for errors in the surveying phase and in the peak discharge estimation, or in the hydrological modelling application. For catchments smaller than 10 km^2, the four sites 37, 12, 25 and 26 are all inconsistent, as defined above. Moreover, among the catchments with size larger than 10 km^2, sites 3 and 6 are flagged as inconsistent. This shows once more that the uncertainties increase with decreasing the size of the catchment. Sites flagged as inconsistent will be revised in a follow-up of this study.

6.3 Influence of rainfall space-time variability on modelled hydrograph properties

To investigate the effect of rainfall space-time variability on modelled hydrograph properties, we carried out a series of hydrologic simulations for which rainfall scenarios with different levels of rainfall variability and zero storm velocity were used. More specifically, the hydrologic response resulting from the original rainfall field (control simulation) was compared with the results obtained from (a) spatially uniform and (b) constant spatial rainfall pattern case. In all cases the basin-averaged rainfall remained constant (i.e. constant rainfall volume applied at each time) while the spatial rainfall pattern was (a) completely removed (in the uniform case) or (b) kept constant and equal to the total rainfall accumulation pattern (constant pattern case). The latter was achieved by scaling the total rainfall pattern with an appropriate factor so that the basin-averaged rainfall remained equal to the original rain. Note that because the overall spatial rainfall organization is preserved in the constant pattern case, the values of Δ_1 and Δ_2 are the same with the control scenario.

The rationale for developing the three rainfall scenarios is as follows. In our methodology, based on spatial moments, we assume that the shape of the flood hydrograph is controlled by: (i) the catchment drainage structure, (ii) the temporal pattern of basin-average rainfall rates (hyetograph); (iii) the two descriptors of overall rainfall

HESSD
8, 10739–10780, 2011

organization at catchment scale Δ_1 and Δ_2, and (iv) the catchment scale storm velocity. The control simulation is the result of the combination of factors (i) to (iv), the constant pattern simulation is controlled by factors (i) to (iii), whereas the uniform-rainfall simulation is controlled by factors (i) and (ii). Comparison of control simulation with constant pattern simulation permits isolation of the effect of catchment scale storm velocity on flood hydrograph, whereas the comparison of control simulation with uniform-rainfall simulation isolates the combined effect of Δ_1, Δ_2, and catchment scale storm velocity on flood hydrograph.

Simulations were carried out for the basin closed at Rangendingen (Fig. 13). Examination of the figure shows that the simulated peak flow increases from uniform rainfall ($107\,m^3\,s^{-1}$) to constant pattern ($127\,m^3\,s^{-1}$) to control scenario ($145\,m^3\,s^{-1}$). This clearly indicates that storm motion is an essential element of space-time rainfall, which play a role in controlling hydrograph shape. Neglecting storm motion, conserving only the shape of the spatial rainfall pattern, leads to underestimating the peak flow by 12 %. The underestimation rises to 26 % assuming a spatially uniform rainfall distribution. These results are consistent with the discussion of Fig. 7 (sign of the peak flow underestimation and hydrograph amplitude agrees). Overall, this shows that the storm velocity played a non-negligible role in shaping the flood hydrograph during this event. It was the combination of the spatial distribution of rainfall volume over the basin and its motion that controlled the flood response.

7 Discussion and conclusions

In this study we have examined the 2 June 2008 extreme flash floods on the Starzel river basin in South-West Germany. The major findings of this work are:

– The Hilal organised system of thunderstorms produced record rainfall and flooding in the Starzel river basin at basin scales ranging from 1 to 30 km^2. The magnitude of the flooding in terms of rainfall rates and unit peak discharge was comparable to that observed in the same region for past extreme events and for other

HESSD
8, 10739–10780, 2011

central European storms producing extreme flooding at these scales. The Hilal event provides a prototype for organized convective systems that dominate the upper tail of the precipitation frequency distribution in the study region as well as in several other contexts in Central Europe.

– The combined approach of hydrological modeling based on rainfall observations and indirect peak discharge estimates based on field survey offers the opportunity to compare peak flow estimates from independent approaches. This greatly helps to validate the results of flood reconstruction and to estimate related uncertainty bounds. This analysis has shown that uncertainty in flood simulation is mainly concentrated at scales less than 10 km^2, due to various sources of uncertainty which include rainfall estimation, structural and parameter uncertainty in the hydrological model and potential errors in indirect peak flow estimation.

– Even though the antecedent soil moisture conditions were relatively wet, small runoff ratios (less than 20 %) characterized the runoff response. These estimates are at the lower range of runoff ratio assessment reported for short-duration events observed in Central Europe (Marchi et al., 2010). Uncertainties in rainfall estimates and model simulations may affect these results. However, these values are in the range of those reported for specific small and medium size catchments and for events characterized by short rain durations in Continental Europe (Zoccatelli et al., 2010).

– The distributed flood response can be reasonably well reproduced with a simple distributed hydrological model, using high resolution rainfall observations and model parameters calibrated at a river section which includes most of the area impacted by the storm. The model is capable of consistently reproducing the flood peaks at 11 sites (out of 17) estimated during the intensive post-flood survey. However, the response at three sites characterized by field-observed extreme response and very small catchment scales proved to be largely underestimated by

HESSD
8, 10739–10780, 2011

the model. The nature of the error (either observational, or on the modeling side, or both) remains elusive.

– The Hilal organized system of thunderstorms was characterized by its rapid storm motion. We developed here a methodology to assess the role of storm motion on modeled flood response. The rapid downbasin motion of the principal rain band was important, even though not dominant, in controlling the magnitude of the runoff response. The orography played a minor role in shaping the spatial distribution of rainfall.

Acknowledgements. This work was financially supported by the EU FP6 STREP Project HYDRATE. Contract GOCE-037024. The post-flood survey was carried out in collaboration with the authorities of Regierungspräsidium Stuttgart, Tübingen and Freiburg as well as the local municipalities of Jungingen and Hechingen. The first author acknowledges the Spanish Ministry of Science and Innovation, for the grant for a 4 months research stay at the University of Padova (Italy), MAS Dendro-Avenidas project and the Geological Survey of Spain and University of Castilla-La Mancha, particularly to Andrés Díez-Herrero and José M. Bodoque for their support and collaboration.

References

Blöschl, G.: Hydrologic synthesis: Across processes, places, and scales, Water Resour. Res., 42, W03S02. doi:10.1029/2005WR004319, 2006.

Borga, M., Anagnostou, E. N., Blöschl, G., and Creutin, J.-D.: Flash flood forecasting, warning and risk management: the HYDRATE project, Environ. Sci. Policy, 14, 834–844, 2011.

Borga, M., Boscolo, P., Zanon, F., and Sangati, M.: Hydrometeorological analysis of the August 29, 2003 flash flood in the eastern Italian Alps, J. Hydromet., 8, 1049–1067. 2007.

Borga, M., Gaume, E., Creutin, J. D., and Marchi, L.: Surveying flash flood response: gauging the ungauged extremes, Hydrol. Processes, 22, 3883–3885, doi:10.1002/hyp.7111, 2008.

Bonnifait, L., Delrieu, G., Lay, M. L., Boudevillain, B., Masson, A., Belleudy, P., Gaume, E., and Saulnier, G.-M.: Distributed hydrologic and hydraulic modelling with radar rainfall input: Re-

HESSD

8, 10739–10780, 2011

construction of the 8-9 September 2002 catastrophic flood event in the Gard region, France, Adv. Water Res., 32, 1077–1089, 2009.

Bouilloud, L., Delrieu, G., Boudevillain, B., and Kirstetter, P. E.: Radar rainfall estimation in the context of post-event analysis of flash-flood events, J. Hydrol., 394, 17–27, doi:10.1016/j.jhydrol.2010.02.035, 2010.

Braud, I., Roux, H., Anquetin, S., Maubourguet, M. M., Manus, C., Viallet, P. and Dartus, D.: The use of distributed hydrological models for the Gard 2002 flash flood event: Analysis of associated hydrological processes, J. Hydrol., 394, 162–181, doi:10.1016/j.jhydrol.2010.03.033, 2010.

Brauer, C. C., Teuling, A. J., Overeem, A., van der Velde, Y., Hazenberg, P., Warmerdam, P. M. M., and Uijlenhoet, R.: Anatomy of extraordinary rainfall and flash flood in a Dutch lowland catchment, Hydrol. Earth Syst. Sci., 15, 1991–2005, doi:10.5194/hess-15-1991-2011, 2011.

Carpenter, T. M., Taylor, S. V., Georgakakos, K. P., Wang, J., Shamir, E., and Sperfslage, J. A.: Surveying Flash Flood Response in Mountain Streams, Eos Trans. AGU, 88, p. 69, doi:10.1029/2007EO060001, 2007.

Costa J. E. and Jarrett, R. D.: An evaluation of selected extraordinary floods in the United States Reported by the US Geological Survey and implications for future advancement of flood science, US Geological Survey, Scientific Investigations Report 2008–5164, 52 pp., 2008.

Delrieu, G., Andrieu, H., and Creutin, J. D.: Quantification of path-integrated attenuation for X- and C-band weather radar systems operating in heavy rainfall, J. Appl. Meteorol., 39, 840–850, 2000.

Delrieu, G., Nicol, J., Yates, E., Kirstetter, P.-E., Creutin, J.-D., Anquetin, S., Obled, Ch., Saulnier, G.-M., Ducrocq, V., Gaume, E., Payrastre, O., Andrieu, H., Ayral, P.-A., Bouvier, C., Neppel, L., Livet, M., Lang, M., Parentdu-Châtelet, J., Walpersdorf, A., and Wobrock, W.: The Catastrophic Flash-Flood Event of 8–9 September 2002 in the Gard Region, France: A First Case Study for the Cévennes–Vivarais Mediterranean Hydrometeorological Observatory, J. Hydrometeorol., 6, 34–52, 2005.

DWD: Deutscher Wetterdienst: Starkniederschlagshöhen für die Bundesrepublik Deutschland – KOSTRA, Offenbach am Main, Eigenverlag des Deutschen Wetterdienstes, 1997.

DWD: Deutscher Wetterdienst: KOSTRA-DWD-2000, Starkniederschlagshöhen für die Bundesrepublik Deutschland (1951–2000) – Fortschreibungsbericht, Offenbach am Main, Eigenverlag des Deutschen Wetterdienstes, 2006.

HESSD

8, 10739–10780, 2011

Gaume, E., Gaál, L., Viglione, A., Szolgay, J., Kohnová, S., and Blöschl, G.: Bayesian MCMC approach to regional flood frequency analyses involving extraordinary flood events at ungauged sites, J. Hydrol., 394, 101–117, doi:10.1016/j.jhydrol.2010.01.008, 2010.

Gaume, E., Bain, V., Bernardara, P., Newinger, O., Barbuc, M., Bateman, A., Blaškoviová, L., Blöschl, G., Borga, M., Dumitrescu, A., Daliakopoulos, I., Garcia, J., Irimescu, V., Kohnova, S., Koutroulis, A., Marchi, L., Matreata, S., Medina, V., Preciso, E.,Sempere-Torres, D., Stancalie, G., Szolgay, J., Tsanis, I., Velasco, D., and Viglione, A.: A collation of data on European flash floods, J. Hydrol., 367, 70–78, doi:10.1016/j.jhydrol.2008.12.028, 2009.

Gaume, E. and Borga, M.: Post flood field investigations after major flash floods: proposal of a methodology and illustrations, Journal of flood risk management, 1, 175–189, doi:10.1111/j.1753-318X.2008.00023.x, 2008.

Hicks, N. S., Smith, J. A. , Miller, A. J., and Nelson, P. A.: Catastrophic flooding from an orographic thunderstorm in the central Appalachians, Water Resour. Res., 41, W12428, doi:10.1029/2005WR004129, 2005.

Lumbroso, D. and Gaume, E.: Reducing the uncertainty in indirect estimates of extreme flash flood discharges, Journal of Hydrology, Available online 1 September 2011, ISSN 0022-1694, doi:10.1016/j.jhydrol.2011.08.048, 2011.

Marchi, L., Borga, M., Preciso, E., and Gaume, E.: Characterisation of selected extreme flash floods in Europe and implications for flood risk management, J. Hydrol., 394, 118–133, doi:10.1016/j.jhydrol.2010.07.017, 2010.

Marchi, L., Borga, M., Preciso, E., Sangati, M., Gaume, E., Bain, V., Delrieu, G., Bonnifait, L., and Poganik, N.: Comprehensive post-event survey of a flash flood in Western Slovenia: observation strategy and lessons learned, Hydrol. Processes, 23, 3761–3770, doi:10.1002/hyp.7542, 2009.

Norbiato, D., Borga, M., Degli Esposti, S., Gaume, E., and Anquetin, S.: Flash flood warning based on rainfall thresholds and soil moisture conditions: An assessment for gauged and ungauged basins, J. Hydrol., 362, 274–290, 2010.

Ogden, F. L., Richardson, J. R., and Julien, P. Y.: Similarity in catchment response: 2. Moving rainstorms, Water Resour. Res., 31, 1543–1547, 1995.

Ogden, F. L. and Saghafian, B.: Green and Ampt infiltration with redistribution, Journal of Irrigation and Drainage Engineering, 123, 386–393, 1997.

Parajka, J., Kohnová, S., Bálint, G., Barbuc, M., Borga, M., Claps, P., Cheval, S., Gaume, E., Hlavová, K., Merz, R., Pfaundler, M., Stancalie, G., Szolgay, J., and Blöschl, G.: Seasonal

HESSD

8, 10739–10780, 2011

characteristics of flood regimes across the Alpine-Carpathian range, J. Hydrol., 394, 78–89, doi:10.1016/j.jhydrol.2010.05.015, 2010.

Smith, J. A., Baeck, M. L., Ntelekos, A. A., Villarini, G., and Steiner, M..: Extreme rainfall and flooding from orographic thunderstorms in the central Appalachians, Water Resour. Res., 47, W04514, doi:10.1029/2010WR010190, 2011.

Versini, P.-A., Gaume, E., and Andrieu, H.: Application of a distributed hydrological model to the design of a road inundation warning system for flash flood prone areas, Nat. Hazards Earth Syst. Sci., 10, 805–817, doi:10.5194/nhess-10-805-2010, 2010.

Zanon, F., Borga, M., Zoccatelli, D., Marchi, L., Gaume, E., Bonnifait, L., and Delrieu, G.: Hydrological analysis of a flash flood across a climatic and geologic gradient: the September 18, 2007 event in Western Slovenia, J. Hydrol., 394, 182–197, doi:10.1016/j.jhydrol.2010.08.020, 2010.

Zoccatelli, D., Borga, M., Viglione, A., Chirico, G. B., and Blöschl, G.: Spatial moments of catchment rainfall: rainfall spatial organisation, basin morphology, and flood response, Hydrol. Earth Syst. Sci. Discuss., 8, 5811–5847, doi:10.5194/hessd-8-5811-2011, 2011.

HESSD

8, 10739–10780, 2011

Table 1. Peak discharge estimates from the field survey. Section reference numbers are reported in Fig. 1.

Ref.	Watershed area (km^2)	Mean flow velocity ($m\,s^{-1}$) (central value)	Peak discharge (central value) ($m^3\,s^{-1}$)	Peak discharge (uncertainty range) ($m^3\,s^{-1}$)
1	9.5	2.8	9.	6.–12.
3	53.9	2.3	150.	130.–170.
4	119.8	2.5	150.	125.–175.
6	47.4	3.7	120.	105.–135.
7	85.7	2.6	165.	150.–180.
10	1.0	1.5	3.5	3.–4.
12	1.1	1.4	6.5	6.–7.
14	26.0	2.4	23.	20.–26.
15	29.0	2.5	33.	28.–38.
16	29.4	2.9	45.	35.–55.
22	33.2	3.3	65.	53.–77.
24	37.6	2.3	90.	70.–110.
25	2.2	3.0	8.	6.–10.
26	2.1	2.5	25.	20.–30.
32	1.1	2.5	3.0	1.5–4.
33	17.8	3.4	20.	15.–25.
37	1.9	2.6	11.	8.–14.

HESSD
8, 10739–10780, 2011

Table 2. Water balance elements for the basin at Rangendingen and at Jungingen (analysis based on the hydrological model application).

Basin	Area	Rain (mm)	Runoff (mm)	Peak discharge ($m^3 s^{-1}$)	Unit peak discharge ($m^3 s^{-1}/km^2$)	Runoff ratio
Rangendingen	120.0	85.6	10.9	146.0	1.21	0.13
Jungingen	33.2	87.8	14.4	60.0	1.81	0.16

HESSD
8, 10739–10780, 2011

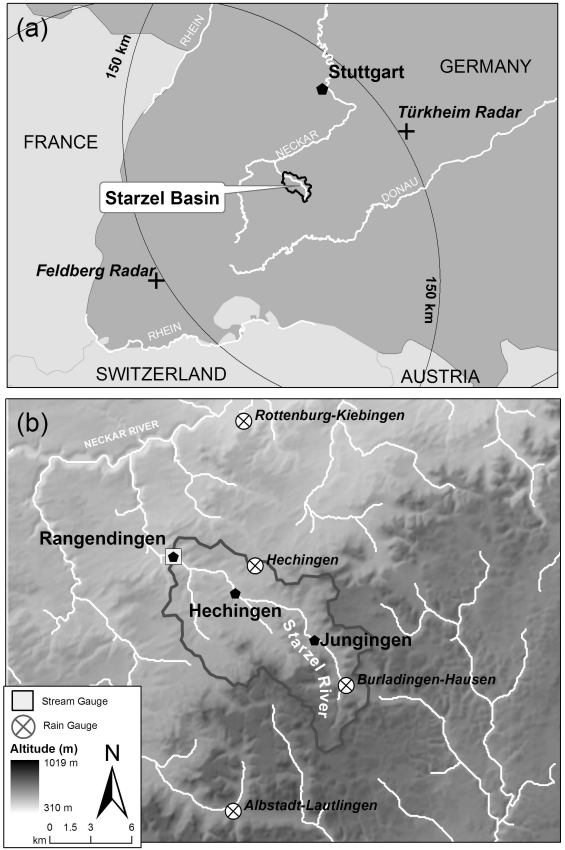

Fig. 1. (a) Location of the Starzel basin with the two weather radars, Türkheim and Feldberg (crosses) and corresponding 150 km range circles; **(b)** the basin with orography and the location of the four raingauge stations and of the streamgauge.

HESSD
8, 10739–10780, 2011

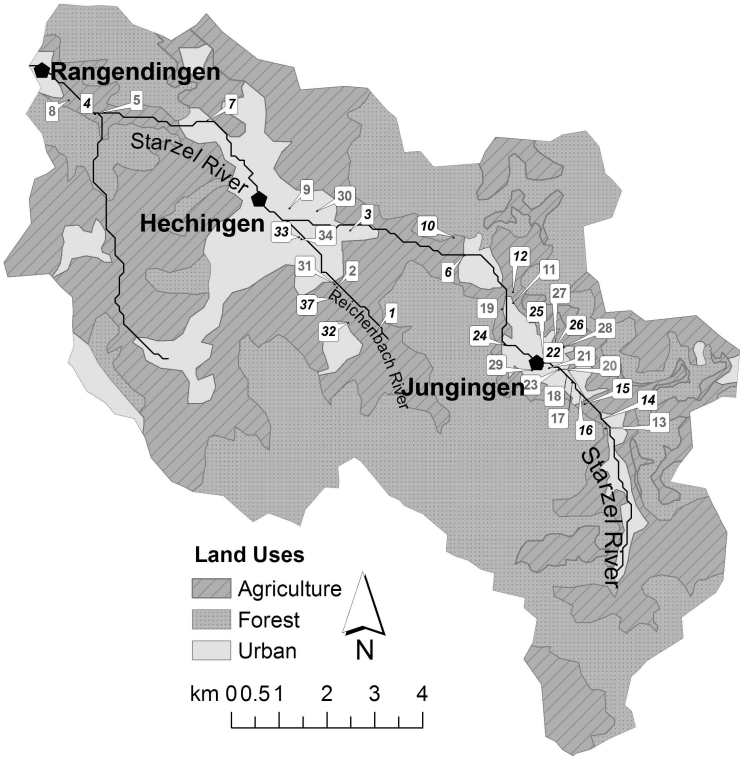

Fig. 2. Land uses map of the Starzel catchment. Numbers refer to the surveyed cross sections during the intensive post event campaign; the 17 sections considered for the study are marked in bold.

HESSD
8, 10739–10780, 2011

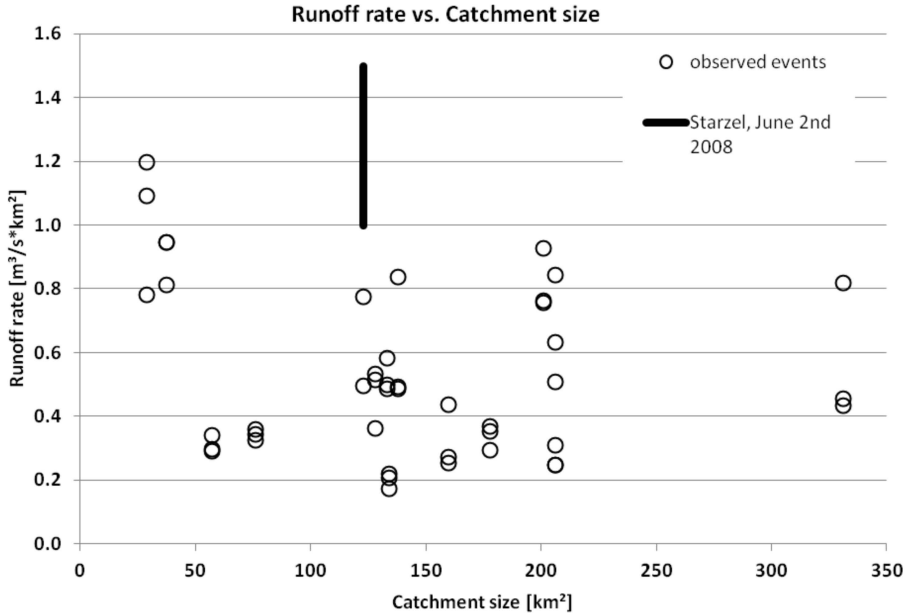

Fig. 3. Unit peak discharges vs. catchment size for the three highest observed peak floods observed in 15 catchments in the Neckar river system near the Starzel. The uncertainty range corresponding to the Starzel flash flood peak estimated in Rangendingen is also reported.

HESSD
8, 10739–10780, 2011

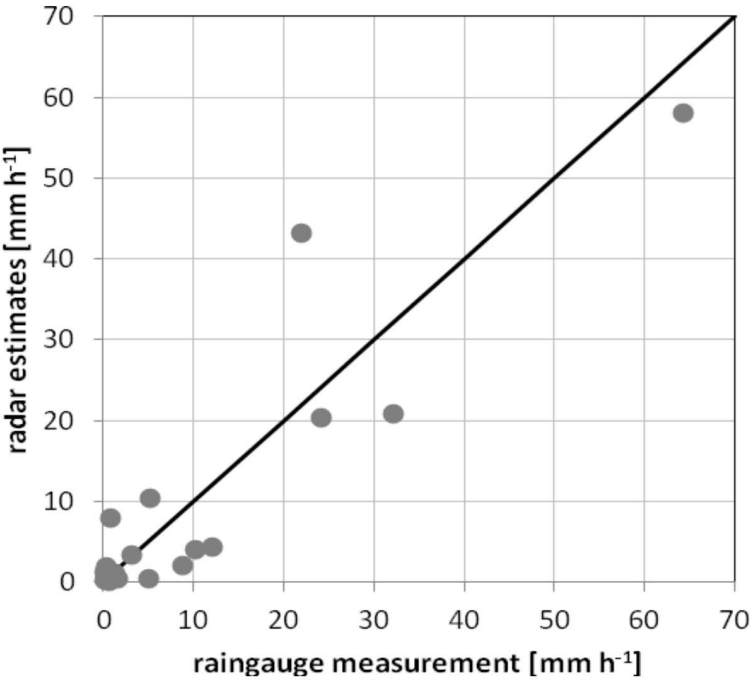

Fig. 4. Scatter plot of adjusted radar rainfall estimates versus raingauges measurements for hourly accumulations.

HESSD
8, 10739–10780, 2011

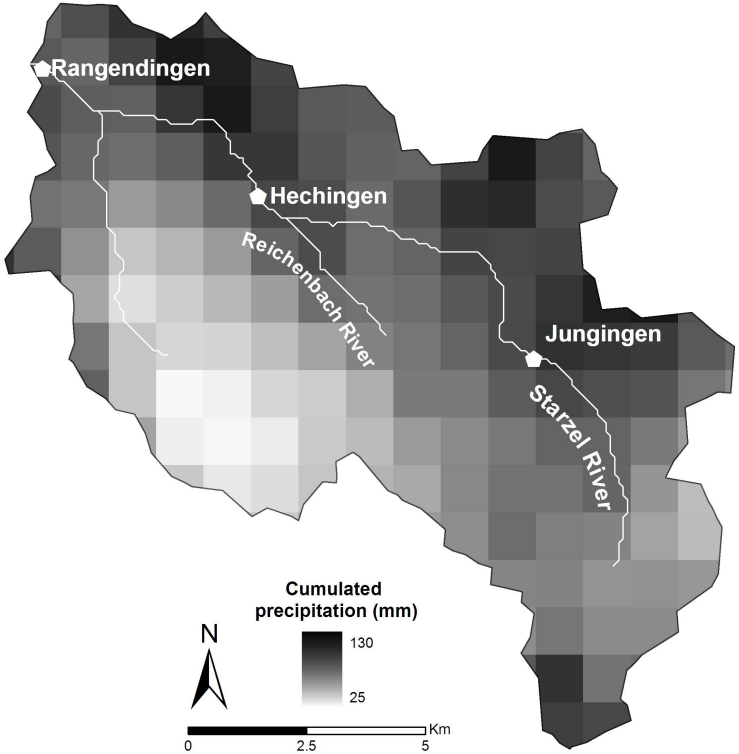

Fig. 5. Event rainfall spatial distribution over the catchment.

HESSD
8, 10739–10780, 2011

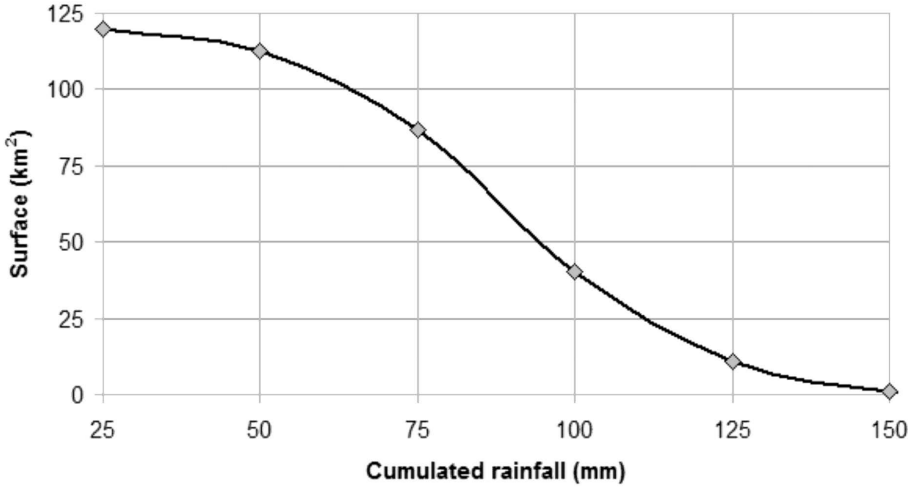

Fig. 6. Distribution of exceedance areas, i.e. the areas over which the event-cumulated rainfall exceeded various thresholds.

HESSD
8, 10739–10780, 2011

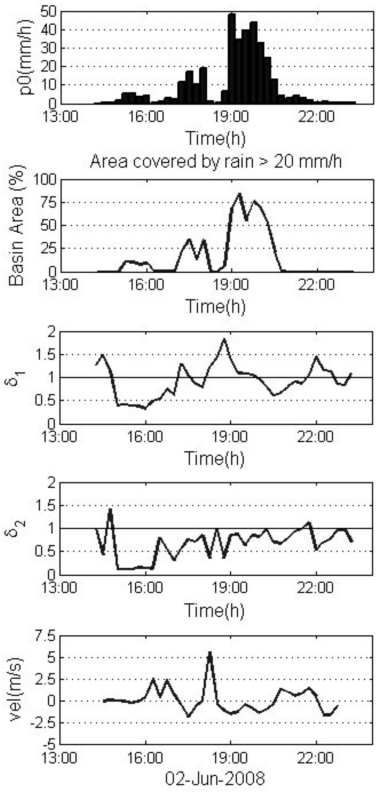

Fig. 7. Precipitation analyses by using 15-min time series of **(a)** precipitation intensity, **(b)** percent coverage of the catchment (for precipitation intensity >20 mm h^{-1}), **(c)** δ_1, **(d)** δ_2, **(e)** catchment scale storm velocity.

HESSD
8, 10739–10780, 2011

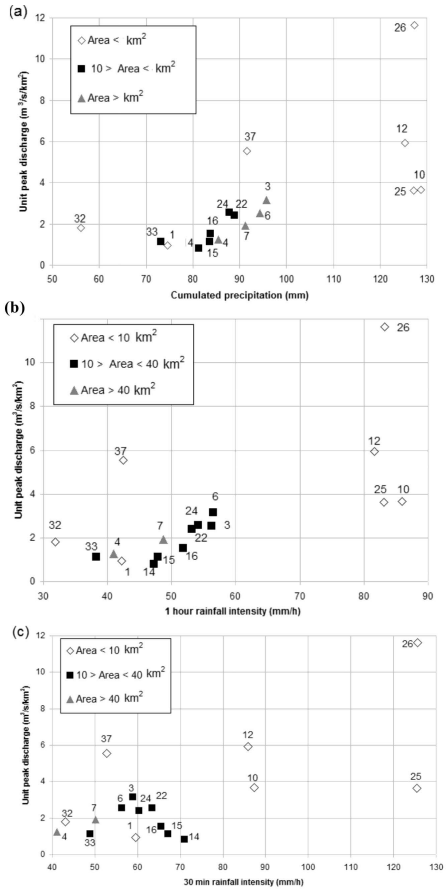

Fig. 8. (a, b, c) Relationship between estimated unit peak discharges and rainfall characteristics for the 17 IPEC catchments: **(a)** event cumulated rainfall; **(b)** max hourly rainfall intensity; **(c)** 30 min maximum rainfall intensity. The numbers refer to the basins listed in Table 1.

HESSD
8, 10739–10780, 2011

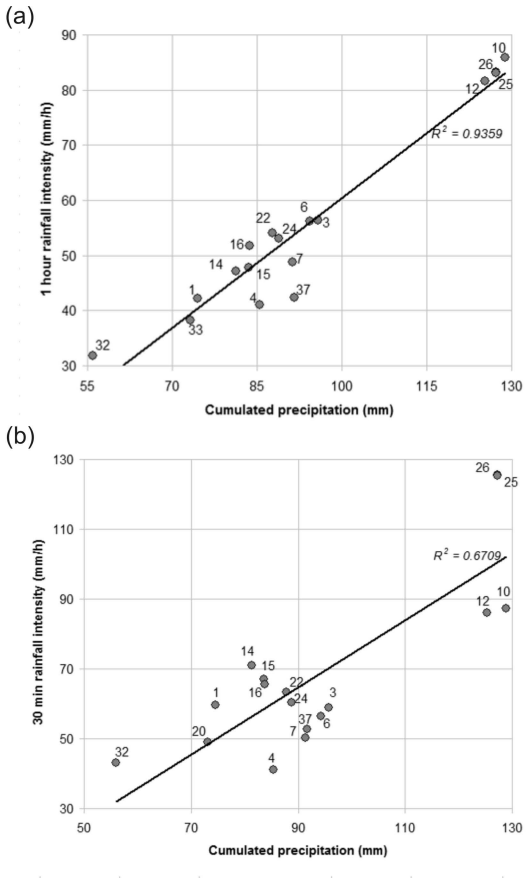

Fig. 9. (a, b) Relationship between the event-cumulated rainfall depth and the 1-h (up) and 30-min peak rainfall intensity (down) for the17 IPEC catchments.

HESSD
8, 10739–10780, 2011

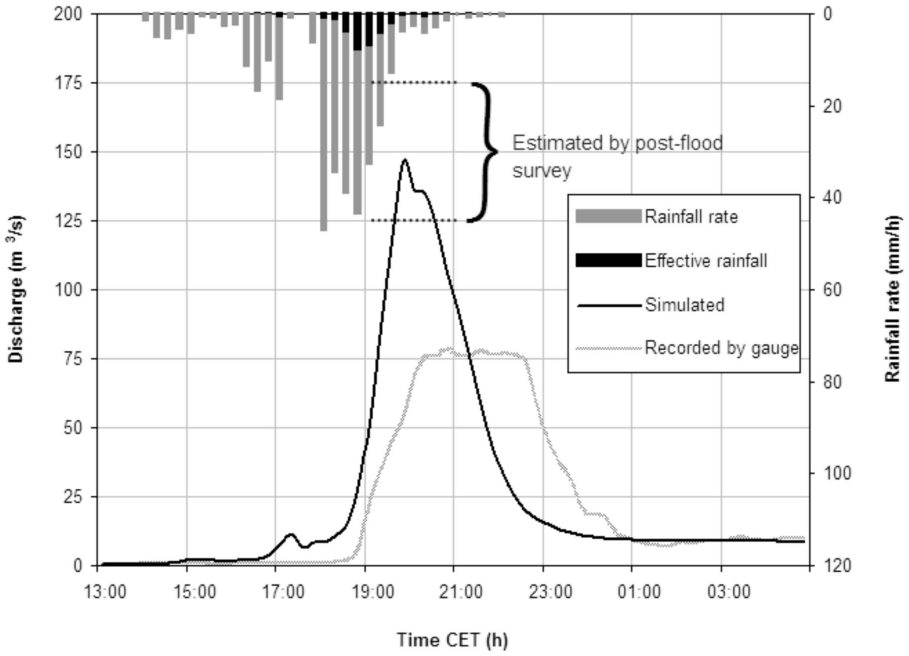

Fig. 10. Hydrograph analysis at the Rangendingen stream gauge station: model-based hydrograph is compared with estimated hydrograph from recorded stages (reconstructed) and with peak flow estimates from post-event survey.

HESSD
8, 10739–10780, 2011

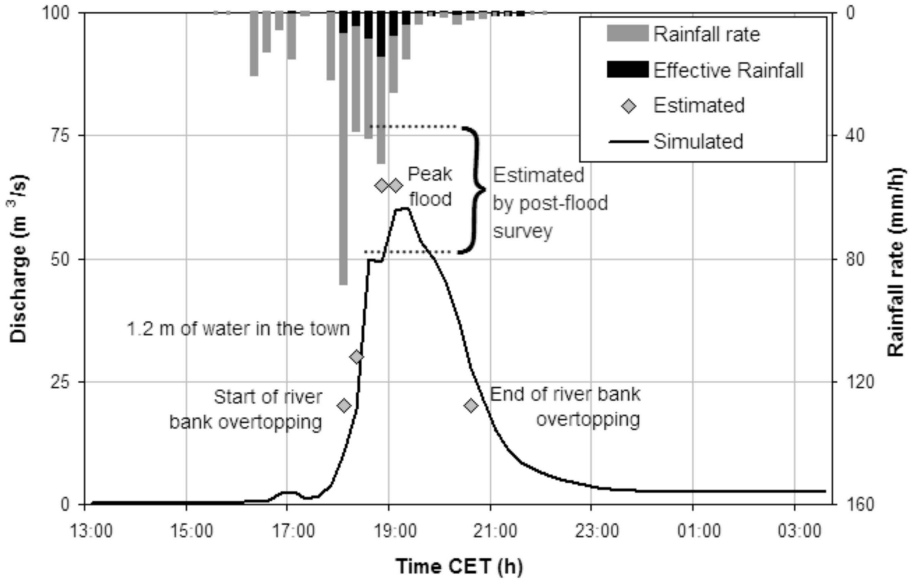

Fig. 11. Flood hydrograph simulation in Jungingen. The diamonds indicate the reported timing of flooding features from eye-witnesses.

HESSD
8, 10739–10780, 2011

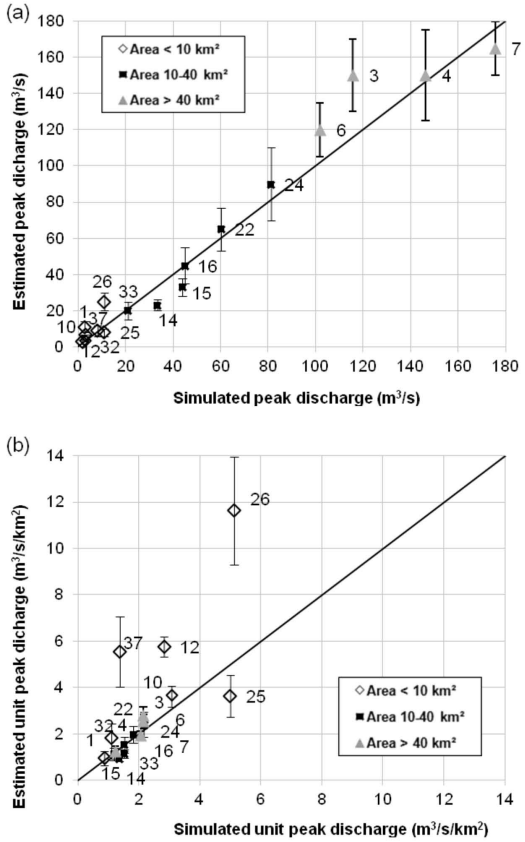

Fig. 12. **(a, b)** Result from runoff model applications over the 17 selected catchments, by considering uncertainty ranges in indirect peak discharge estimation: **(a)** estimated versus simulated peak discharges; **(b)** estimated versus simulated unit peak discharges. Nash Sutcliffe efficiency statistics are 0.92 and 0.45, respectively.

HESSD
8, 10739–10780, 2011

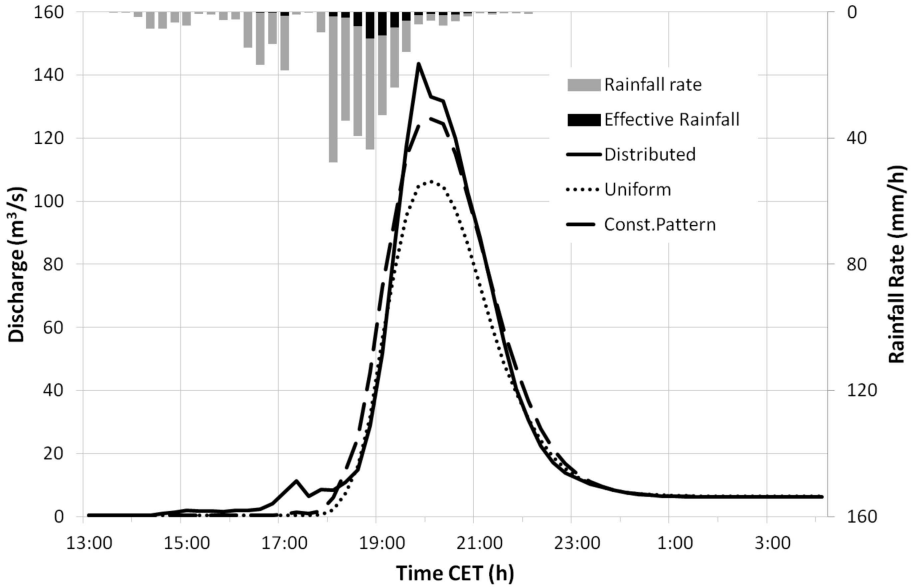

Fig. 13. Hydrograph analysis at the Rangendingen stream gauge station: resulting model-based hydrographs by using control rainfall (Distributed), spatially uniform rainfall (Uniform) and constant spatial pattern (Const. Pattern).

HESSD
8, 10739–10780, 2011